Article

Enantioselective hydroformylation by a Rh-catalyst entrapped in a supramolecular metallocage

Cristina García-Simón, Rafael Gramage-Doria, Saeed Raoufmoghaddam, Teodor Parella, Miquel Costas, Xavi Ribas, and Joost N. H. Reek

J. Am. Chem. Soc., **Just Accepted Manuscript** • DOI: 10.1021/ja512637k • Publication Date (Web): 29 Jan 2015

Enantioselective hydroformylation by a Rh-catalyst entrapped in a supramolecular metallocage

Cristina García-Simón,[a] Rafael Gramage-Doria,[b] Saeed Raoufmoghaddam,[b] Teodor Parella,[c] Miquel Costas,[a]* Xavi Ribas,[a]* Joost N. H. Reek[b]*

a) Grup de Química Bioinorgànica i Supramolecular (QBIS). Institut de Química Computacional i Catàlisi (IQCC) and Departament de Química, Universitat de Girona. Campus Montilivi, E17071 Girona, Catalonia (Spain) xavi.ribas@udg.edu, miquel.costas@udg.edu

b) Servei de RMN, Facultat de Ciències, Universitat Autònoma de Barcelona, Campus UAB, Bellaterra E-08193, Catalonia, Spain.

c) Homogeneous and Supramolecular Catalysis Group, Van't Hoff Institute for Molecular Science (HIMS), University of Amsterdam (UvA), Science Park 904, 1098 XH Amsterdam (The Netherlands) J.N.H.Reek@uva.nl

Abstract

Regio and enantioselective hydroformylation of styrenes is described upon embedding a chiral Rh complex in a non-chiral supramolecular cage formed from coordination-driven self-assembly of macrocyclic dipalladium complexes and tetracarboxylate zinc porphyrins. The supramolecular catalyst that results converts styrene derivatives into aldehyde products with much higher chiral induction in comparison to the non-encapsulated Rh catalyst. Spectroscopic analysis shows that encapsulation does not change the electronic properties of the catalyst, nor changes its first coordination environment. Instead, enhanced enantioselectivity is rationalized by the modification of the second coordination sphere occurring upon catalyst inclusion inside the cage, being one of the few examples in achieving enantioselective outcome via indirect through-space control of the chirality around the catalyst center. This effect resembles those taking place in enzymatic sites, where structural constrains imposed by the enzyme cavity can impart stereoselectivities that cannot be attained in bulk. These results are a showcase for the future development of asymmetric catalysis by using size-tunable supramolecular capsules.

Introduction

Reactions taking place at enzyme active sites generally exhibit high rates and exquisite selectivities that differ from those occurring in bulk solution. This is best exemplified in asymmetric catalysis. Weak interactions with aminoacid residues precisely modulate the relative orientation of reagents and in some cases assist in their activation.[1] The orientation of the reagents and substrates are controlled by the special environment around the active site leading to highly selective transformations. As such, structural constrains and weak interactions conspire in decreasing activation barriers of precise reactions to furnish rapid, chemo, regio and stereoselective transformations.[2-14] In analogy to the spatial constrains imposed by enzyme active sites metal based catalysts have been included in molecular nanovessels,[15-21] with the aim to modulate their activity and selectivity via the second coordination sphere. High chemo and regio selectivities have been obtained in selected cases, but the number of stereoselective transformations carried out in molecular cages remains scarce.[2-3, 22-27,28] Furthermore, a common limitation of this kind of supramolecular catalysts is that selectivity is most often built at the expenses of decreasing reaction rates.

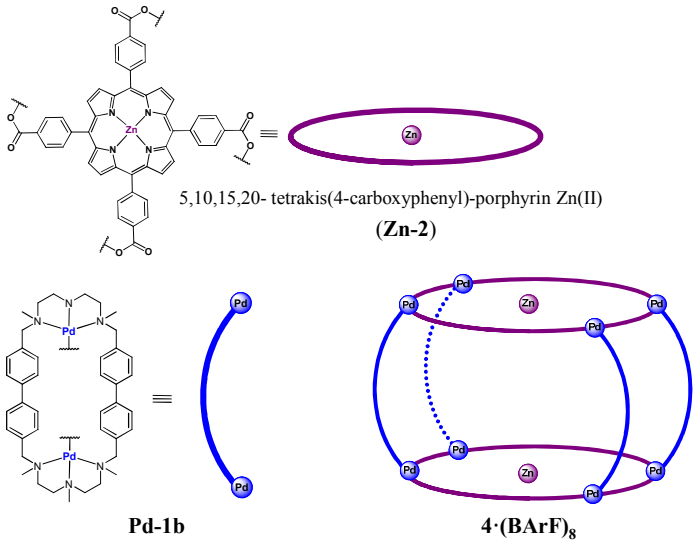

Scheme 1. Schematic representation of the building blocks used in the synthesis of tetragonal-prismatic nanocapsule **4**·(BArF)$_8$.

A template ligand approach to form encapsulated ligands and their metal complexes were previously described, and demonstrated that regioselectivity in hydroformylation reactions can be controlled by the second coordination sphere.[29-32] Generally this strategy results in exclusive monoligated rhodium complexes that are very reactive. For asymmetric hydroformylation some of us recently extended the approach to chiral phosphoramidite,[10,12] but the monoligated complexes generally resulted in low to moderate enantioselectivity. By using bis-zinc(II)salphen building blocks, the ligand-template approach resulted in the formation of bis-ligated rhodium

complexes, embedded in a well-defined cavity.[14] Although the enantioselectivity induced by this complex was high, the activity was rather low, especially at room temperature.

Here we use a different strategy that consists of encapsulating the mono-phosphoramidite-Rh(I) catalysts[10-14] in a tetragonal cage that was previously prepared by metal directed self-assembly.[33] The resulting monoligated catalyst confined within the cavity of the capsule, is especially active in hydroformylation of styrene and derivatives, and provides good levels of steroselectivity. Chiral induction is greatly enhanced in comparison to the non-encapsulated analogue. These observations provide compelling evidence that steroselectivity provided by these catalysts is based in controlling the second coordination sphere by reason of the structural constrains imposed by the cage.

Results and discussion

Host-guest experiments. Some of us have previously described the synthesis of the tetragonal prismatic nanocage **4**·$(BArF)_8$, which shows high affinity for fullerenes from C_{60} to C_{84}.[33] This property has been used in the selective separation of C_{60} from mixtures of fullerenes. Cage **4**·$(BArF)_8$ is based on two opposing Zn-porphyrin building blocks, linked by four bridging macrocyclic walls that assemble the cage structure through Pd-carboxylate coordination bonds (Scheme 1).

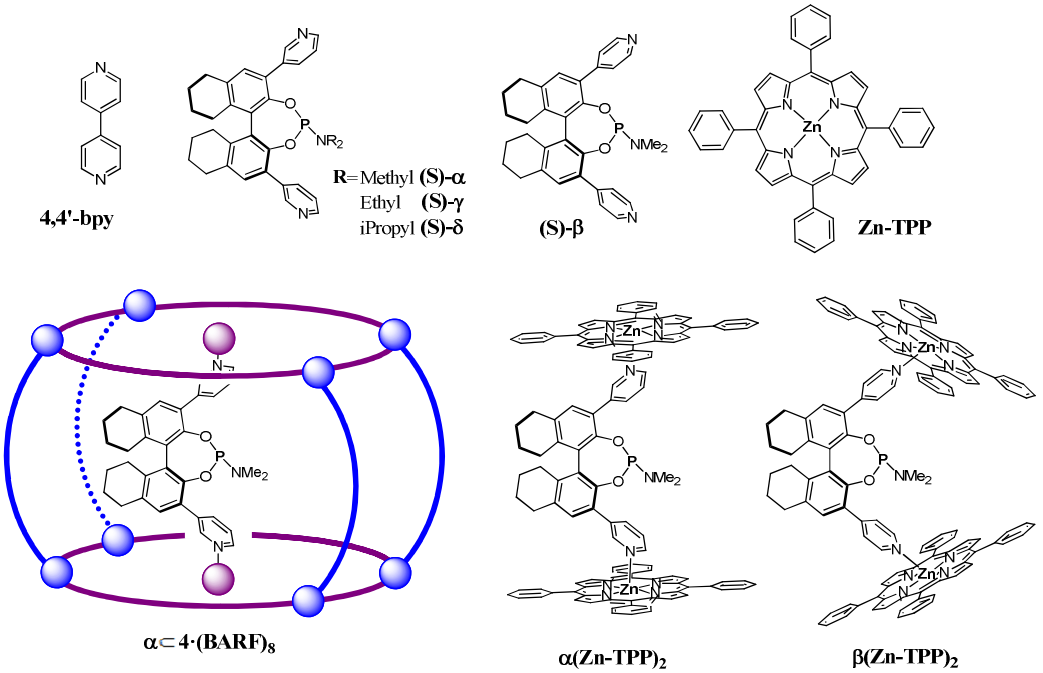

Scheme 2. Zn^{II}-template (**Zn-TPP**) and mono-phosphoramidite ligands (**α**, **β, γ, δ**) used in this study. Structure of host-guest **α**⊂**4**·$(BArF)_8$ cage structure and ligand-template systems **α**(**Zn-TPP**)$_2$ and **β**(**Zn-TPP**)$_2$.

We envisioned that cage **4**·$(BArF)_8$ would be able to accommodate pyridine-based ligands due to the well-known ability of Zn-porphyrins to interact with pyridine moieties.[8-14, 34] We first sought to prove this by using 4,4'-bipyridine (**4,4'-bpy**) as guest since we have shown that the Zn···Zn porphyrin distance of **4**·$(BArF)_8$ can vary from ~11-14 Å (Scheme 2), owing to the structural flexibility of Pd-carboxylate bonds.[33]

As anticipated, UV-vis titration experiments unambiguously indicated an interaction between the nanocapsule and **4,4'-bpy**. High resolution mass spectrometry (HR-MS) analysis as well as ^{1}H NMR experiments of the host-guest compound indicated the formation of **4,4'-bpy**⊂**4**·$(BArF)_8$ adduct in a 1:1 stoichiometry (see Experimental Section and Figures S1-4 in the Supporting Information).

The geometry of the **4,4'-bpy**⊂**4**·$(BArF)_8$ adduct was fully characterized by means of 1D and 2D NMR spectroscopy (see Figures S5-8). At room temperature, the ^{1}H-NMR spectrum exhibited some moderate upfield shifts in the signals corresponding to some of the aromatic protons of the cage. Additionally, an isolated strongly upfield shifted doublet signal centered at 4.91 ppm corresponding to the **4,4'-bpy** was observed (see Figure S5a). 2D COSY and ^{1}H-^{13}C HSQC spectra confirmed that the **4,4'-bpy** signals (resonate at 4.91/120.4 and 2.23/142.2 ^{1}H/^{13}C ppm) experience a strong upfield chemical shift effect upon encapsulation, due to the anisotropic ring currents from the porphyrin moieties. The stronger effect on proton **a** is a consequence of its very close proximity to the aromatic rings from the porphyrin (see Figure 1a). The **4,4'-bpy** nitrogen chemical shift was also expected to be a good indicator of the encapsulation, since it will also be altered by the porphyrin rings electron density.[35-36] Therefore ^{1}H-^{15}N HMBC spectra of free and encapsulated **4,4'-bpy** were recorded. A chemical shift from 319.5 ppm (**4,4'-bpy**) to 274.6 ppm (**4,4'-bpy**⊂**4**·$(BArF)_8$) further confirmed the coordination of the N atoms from the bpy to the Zn(II)-porphyrins (see Figure S7-8). DOSY-2D NMR experiments also supported the formation of the **4,4'-bpy**⊂**4**·$(BArF)_8$ 1:1 host-guest adduct (see Section 1.4 in the Supplementary Information and Figure S9).

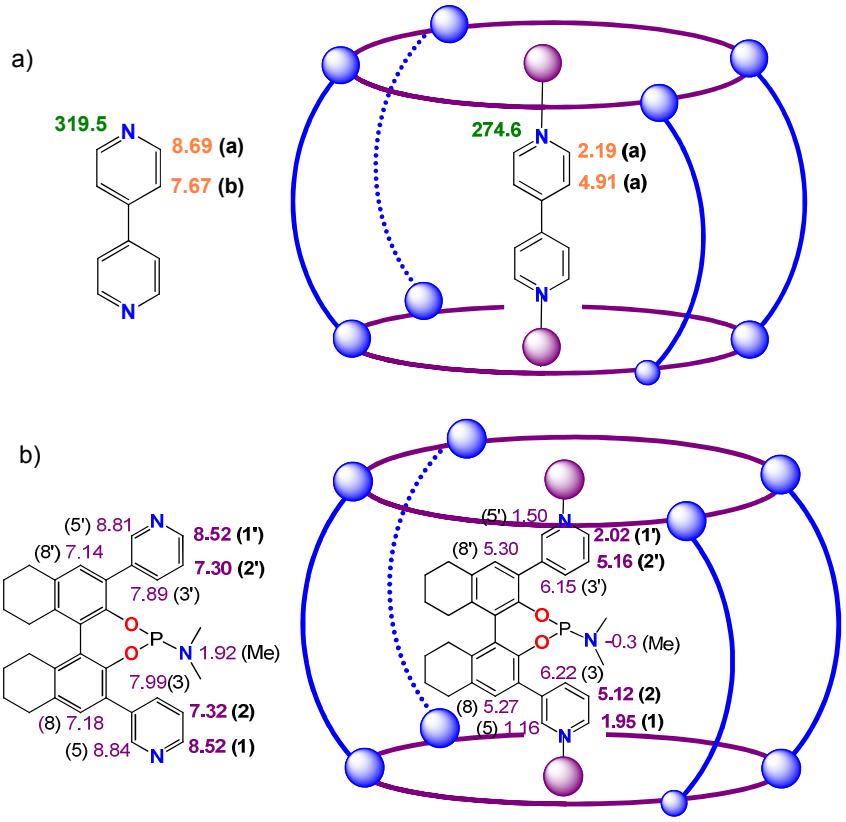

Figure 1. a) ^{1}H-NMR and ^{15}N-NMR assignment of free and encapsulated **4,4'-bpy** (experiments were performed in CD_3CN at 298 K). **b)** ^{1}H-NMR assignment of free and encapsulated ligand **α** (experiments were performed in CD_3CN at 298 K and 243 K respectively). See the corresponding spectra in the supplementary information.

The next step was the inclusion of phosphoramidite (S)-**α** within **4**·$(BArF)_8$ cage with the aim of preparing *in situ* the encapsulated Rh-catalysts to be then employed in asymmetric hydroformylation reactions. We envisioned that the $N_{pyr}\cdots N_{pyr}$ distance in **α** (~11 Å) might be suitable to fit inside **4**·$(BArF)_8$, whereas ligand **β** (containing pyridine groups in *para* position) does not have a suitably orientation to bind with both pyridyl groups simultaneously to the porphyrin units of the cage. The UV-Vis titration between capsule **4**·$(BArF)_8$ and ligand **α**, displayed a bathochromic shift of the Soret band from the porphyrins, exhibiting two isosbestic points, suggesting the formation of a 1:1 host-guest adduct (see Figure 2a-b). The 1:1 interaction was further confirmed by Job's Plot analysis (see Figure 2c). From the UV-Vis data a binding constant of $(3.6 \pm 0.2)\cdot 10^6$ M^{-1} was obtained. This high binding constant can be illustratively compared to that observed for **α**(**Zn-TPP**)$_2$ (K_a *ca.* 10^3 M^{-1}), strongly suggesting that **α** is indeed bound in a ditopic fashion within **α**⊂**4**·$(BArF)_8$.[10] As a consequence, the phosphoramidite ligand is located in the middle of the supramolecular cage. HRMS experiments also supported the formation of **α**⊂**4**·$(BArF)_8$ (see Figure S10). As anticipated, ligand **β** is not encapsulated within nanocapsule **4**·$(BArF)_8$, as shown by UV-vis studies (see Figure S11).

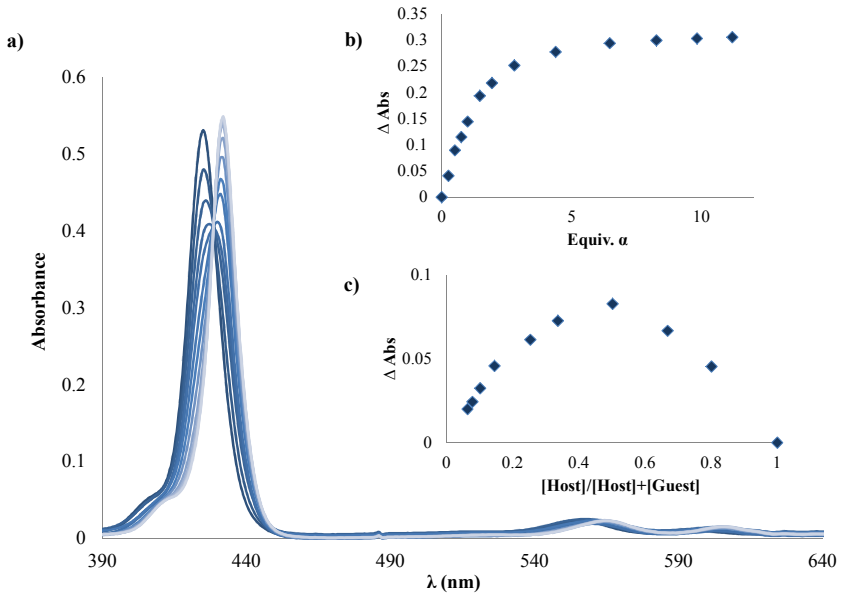

Figure 2. a) UV-Vis monitoring of the titration of **4**·$(BArF)_8$ nanocapsule with ligand **α**, at a fixed total concentration ($4.32 \cdot 10^{-7}$ M) of nanocapsule **4**·$(BArF)_8$ in Toluene/CH_3CN (9/1). b) Absorbance variation at the Soret band versus different concentrations of the ligand. **c)** Job's plot showing a 1:1 stochiometry for the host-guest complex of the nanocage **4**·$(BArF)_8$ and ligand **α**.

The ^{1}H-NMR characterization of **α**⊂**4**·$(BArF)_8$ displayed similar trends than the analogous ones corresponding to **4,4'-bpy**⊂**4**·$(BArF)_8$ (see Figures S12-17). The ^{1}H-NMR spectrum of the **α**⊂**4**·$(BArF)_8$ adduct in acetonitrile at 298 K exhibited some line broadening effects for all $BArF^-$ signals whereas smaller and very broad signals were observed for the encapsulated ligand (between 5-6.5 ppm) and the capsule. The broad signals might evidence some complex dynamic process and loss of symmetry of the host-guest adduct in comparison with the highly symmetric structure of empty **4**·$(BArF)_8$. In addition, a broad upfield shifted signal was observed at -0.3 ppm. In order to try to simplify the spectrum, it was recorded at 243 K. In the latter spectrum the signals became sharper and suitable to be studied by 2D NMR methods. 2D COSY, NOESY and HSQC spectra recorded at 243 K allowed us to identify and assign most of the signals belonging to encapsulated ligand **α** (see Figure 1b). Compared to the free ligand, all ^{1}H signals corresponding to confined **α** appeared doubled at 243 K, confirming that the ligand is not symmetric when bound to the nanocage. Moreover, very pronounced upfield effects are observed for all pyridine aromatic protons from ligand **α** (resonating around 1-2 ppm), in strong agreement with the trends observed for the model **4,4'-bpy** substrate. The three spin proton systems belonging to the pyridine rings of **α** (protons labeled as 1,1',2,2',3,3',5,5',8,8' see Figures 1b and S15), were quickly assigned from the evident COSY and NOE cross-peaks, and their ^{13}C chemical shifts assigned by HSQC. Protons 8 and 8' which appeared as two separated singlets at 5.30 and 5.27 ppm were assigned by the NOE enhancement with the aromatic proton resonating at 1.50/1.16 ppm, respectively. The N-methyl signals were assigned to the signal at -

0.3 ppm, from the NOEs with the surrounding protons observed in the NOESY spectrum (see Figure S16).

Interestingly, the ^{31}P-NMR exhibited a singlet at ≈ 137.0 ppm, similar to the free ligand **α**, indicating that the phosphorus is not coordinated to any of the metals of **4**·(BArF)$_8$, and therefore remains available for coordination to the rhodium-metal center that is used for catalysis (see Figure S18).

In conclusion, the sum of the spectroscopic data led to the conclusion that **α** is encapsulated and is strongly bound to **4**·(BArF)$_8$. Furthermore, this binding did not involve the phosphine atom, which remains available for binding the Rh ion.

Preparation of the encapsulated catalyst. The Rh(I) catalyst was formed *in-situ* by addition of 1 eq of [Rh(acac)(CO)$_2$] to a deuterated toluene/acetonitrile (5/2 *v/v*)[6] solution of **α**⊂**4**·(BArF)$_8$ (Scheme 3). Key features of the rhodium complex have been identified by IR and NMR spectroscopy (see Figures S19-20). The carbonyl vibration of the CO ligand was detected by IR spectroscopy (ν = 1995 cm^{-1}) (see Figure S21). The ^{31}P-NMR displays a typical doublet centered at δ = 147 ppm, with a phosphorus rhodium coupling ($^1J_{P\text{-}Rh}$= 260 Hz) suggesting the formation of monoligated species (see Scheme 3).[10]

Under catalytic conditions (5 bar of H$_2$/CO 1:1), the rhodium acac precursor was converted into the typical hydride species, in this case the [*trans*-Rh(H)(CO)$_3$**α**⊂**4**·(BArF)$_8$] was observed. High Pressure (HP) ^{1}H NMR spectrum of [Rh(H)(CO)$_3$-**α**⊂**4**·(BArF)$_8$] shows signals corresponding to the catalyst-capsule adduct (Fig. S22), thus indicating its stability under the catalytic conditions. Moreover, a double doublet centered at -11.7 ppm is observed, indicating formation of the hydride at a monoligated rhodium complex (Scheme 3). The large phosphorus coupling ($J_{H\text{-}P}$= 175.5 Hz) shows that the phosphorus donor atom is located *trans* to the hydride, similar to that observed for [*trans*-Rh(H)(CO)$_3$-**β**(**Zn-TPP**)$_2$].[10-11] The ^{1}H-{^{31}P}-NMR spectrum displays a single peak at -11.9 ppm, confirming that the large coupling is between the phosphorus and the hydride (see Figure S22-S23).

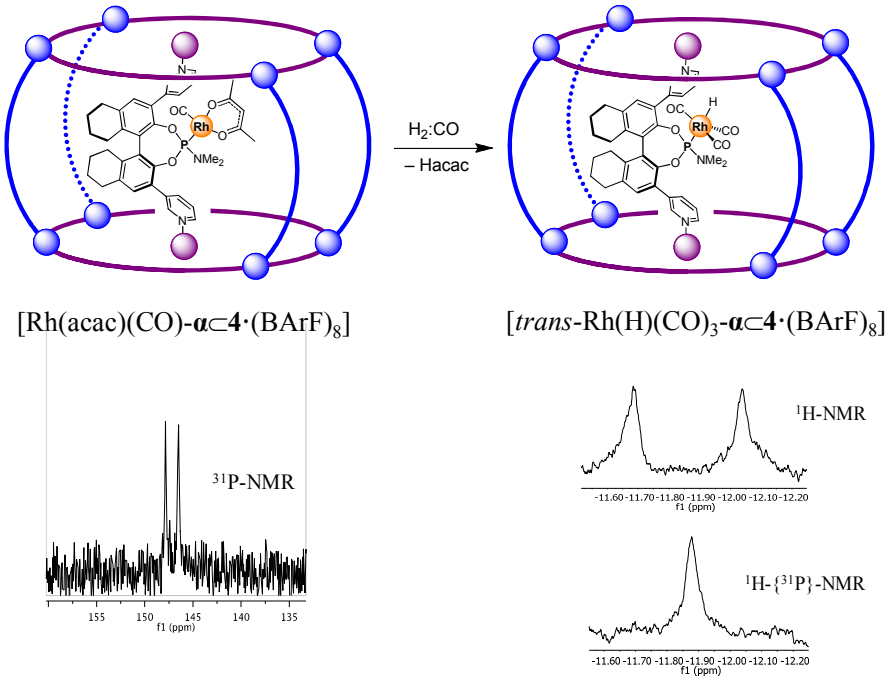

Scheme 3. NMR and High Pressure NMR spectra of [Rh(acac)(CO)-**α**⊂**4**·$(BArF)_8$] and [*trans*-$Rh(H)(CO)_3$-**α**⊂**4**·$(BArF)_8$].

Application of the encapsulated catalyst in asymmetric hydroformylation catalysis. Once the encapsulated Rh catalyst was thoroughly characterized, we focused on the investigation of its catalytic performance in the asymmetric hydroformylation (AHF) of styrene.[37-41] To clearly study the effect of encapsulation, catalytic activities of [Rh(acac)(CO)-**α**⊂**4**·$(BArF)_8$] were compared with that of the Rh-complex of **α**(**Zn-TPP**)$_2$. Due to limited solubility, catalyst loading was kept low at $2 \cdot 10^{-4}$ mol%. As common practice, a five-fold excess of ligand⊂capsule (**α**⊂**4**·$(BArF)_8$) was used in all the experiments in order to avoid the formation of ligand-free rhodium species, an active and nonselective catalyst that could compromise the selectivity. Reactions were performed at room temperature, and the turnover numbers and *ee*'s are reported in Tables 1-4.

Table 1. Asymmetric hydroformylation of styrene using Rh-catalysts based on **α⊂4**·$(BArF)_8$ cage structure and ligand-template system **α**(**Zn-TPP**)$_2$.[a]

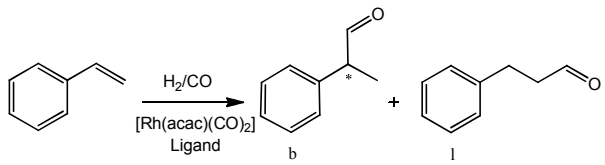

Entry	Ligand	b/l[d]	*ee* (%)[e]	Conv (%)	TON
1	**α⊂4**·$(BArF)_8$	99/1	**74 (R)**	**14**	**797**
2	-	*n.d.*[f]	*n.d.*[f]	<1	<1
3	**α**	99/1	<1	6	342
4	**α(ZnTPP)$_2$**	99/1	9(R)	7	363
5	**4**·$(BArF)_8$	99/1	<1	6	300
6[b]	**α⊂4**·$(BArF)_8$	99/1	65 (R)	32	1600
7[c]	**α⊂4**·$(BArF)_8$	99/1	70 (R)	7	339
8[c]	-	*n.d.*[f]	*n.d.*[f]	<1	<1
9[c]	**α**	99/1	8 (R)	4	197
10[c]	**α(ZnTPP)$_2$**	99/1	16 (R)	4	215
11	**γ⊂4**·$(BArF)_8$	99/1	**79 (R)**	6	**308**
12	**γ**	99/1	7 (R)	3	136
13	**δ⊂4**·$(BArF)_8$	99/1	**77 (R)**	2	**104**
14	**δ**	99/1	6 (R)	1	41

a] Reagents and conditions: [Rh]= 33 μM in toluene/MeCN (4/1), ligand⊂capsule/[Rh(acac)$(CO)_2$]=5, alkene/rhodium=5000, rt, 20 bar, 96 h. Rh Complex: Rh(acac)$(CO)_2$. [b] The catalytically active species is generated under 20 bar of syngas, 16h, 40ºC. Then the styrene was added and the reaction was performed at rt, 20 bar, 96h. [c] [Rh]= 33 μM in toluene/MeCN (2/3), rt, 20 bar, 96 h. [d] Ratio of branched and linear aldehyde. [e] Enantiomeric ratio determined by chiral GC analysis (Supelco BETA DEX 225). [f] *n.d.*= non-detected.

Much to our delight, encapsulated Rh catalyst [Rh(H)$(CO)_3$-**α⊂4**·$(BArF)_8$] gave a higher turnover number (Table 1, entries 1, 6 and 7) than the non-encapsulated analogue (entries 3 and 9) and also than the catalyst based on assembly **α(ZnTPP)$_2$** (entries 4 and 10). As previously observed, when the reaction is carried out with rhodium complex **α** in absence of zinc(II) porphyrins, very low conversion is observed, likely due the presence of free pyridyl groups that compete with the substrate for coordination at the rhodium center. The effect of encapsulation on the selectivity of the reaction was remarkable; when assembly **α**(**Zn-TPP**)$_2$ was used as ligand, a modest 9% *ee* was observed, whereas complete encapsulation of the ligand by using **α⊂4**·$(BArF)_8$ resulted in 74% *ee* (Table 1, entries 1-4). The encapsulated catalyst gives among the highest chemo and stereoselectivities for a monoligated rhodium complex reported so far.[6] Using an incubation period at 40 ºC before initiating the reaction resulted in a higher TON, at the expense of the selectivity (TON from 797 to 1600, *ee* from 74 to 65%; see entries 1 and 6). Further optimization by changing the toluene/acetonitrile ratio did not improve the results

(Table 1, entries 7-10). Remarkably, a control experiment in which capsule **4**·$(BArF)_8$, along with the Rh complex, were used as catalyst provided racemic aldehyde (Table 1, entry 5). Moreover, ^{1}H-NMR experiments were performed in order to see if the nanocapsule still maintains its structure under the high pressure reaction conditions employed in catalytic experiments. Effectively, the cage remains unaltered even after heating a solution of **4**·$(BArF)_8$ at 60 ºC under 5 bar of syngas during 2h (see Figure S24). No precipitate appeared on the NMR tube, strongly suggesting that the capsule is not destroyed under these conditions since the capsule's building blocks are not soluble in DCM. Cage decomposition would have led to the appearance of a precipitate. As a complementary experiment, the reaction crude obtained in one of the catalytic experiments was dried and redissolved in a toluene-d_8/CD_3CN mixture to record the ^{1}H-NMR. The spectrum showed that the integrity of the ligand-cage adduct was still maintained after the catalysis (Fig. S25).

In order to fine tune the supramolecular assemblies and optimize the activity and the selectivity of the catalytic transformation, the Rh-catalyzed AHF of styrene was further studied using ligands **γ** (R=Et) and **δ** (R= *i*Pr) in the presence and the absence of cage **4**·$(BArF)_8$ (Scheme 1 and Table 1, entries 11-14). Replacing ligand **α** for **γ** leads to a slight increase in the *ee* (from 74% to 79%) but at the expense of the activity (TON decreases from 797 to 308). When using ligand **δ** again a small increase in the *ee* was observed (from 74% to 77%) but the activity was drastically lower in comparison with ligand **α**⊂**4**·$(BArF)_8$ (TON from 797 to 104)**.** These results reveal that small modifications to the ligand building block allow optimization of the selectivity and activity of the supramolecular catalysts which opens the door to future catalyst optimization. So far, **α**⊂**4**·$(BArF)_8$ affords the best compromise in *ee* and TON of this new class of encapsulated catalysts for the AHF of styrene.

Preliminary molecular modelling studies were performed (see Figures S26-29) to shine light on the effect of encapsulation in the performance of the Rh catalyst. For the non-encapsulated catalysts ($Rh(H)(CO)_3$-**α**), calculations show that there is a wide space for coordination of the styrene molecule in four orientations to the two available coordination sites that can lead to subsequent selectivity determining hydride migration, which constitutes the key step that ends up determining the enantioselectivity. Since the substrate can approach the catalyst with multiple orientations, the overall stereoselectivity that results when reactions are performed in absence of the cage is poor. In contrast, when the catalyst is docked into the nanocapsule, the cage walls prevent most of the coordination modes of styrene to the Rh center, effectively blocking some of the reaction pathways (Figures S28-29).

Given the promising results obtained in the AHF of styrene, the substrate scope of **α**⊂**4**·$(BArF)_8$ was evaluated using different *para*-R-substituted styrene derivates (R = H, Cl,

CH_3, OCH_3, *t*Bu). The results obtained for these substrates were similar to the ones obtained for styrene (Table 2); in all cases, the best activities were obtained when ligand **α** was encapsulated in cage **α⊂4**·$(BArF)_8$. The conversion (TON) and the regioselectivity depended to some extend on the substituent on the styrene. The selectivity towards the branched aldehyde was maintained when R = *t*Bu (Table 2, entry 17), whereas for R = CH_3 and OCH_3 the b/l ratio was slightly lower (91/9, Table 2, entries 9, 13). For 4-Cl-styrene the selectivity decrease even down to b/l = 80:20 (Table 2, entry 5). In all cases, substrates bearing substituents at position 4 showed a decrease in *ee*. Nevertheless, comparison of these results with those of the **α**(**Zn-TPP**)$_2$ rhodium catalyst consistently showed the benefits of catalyst encapsulation in cage **4**·$(BArF)_8$. In general, *ee*'s are below 12% for **α**(**Zn-TPP**)$_2$ (Table 2, entries 4, 8, 12, 16), but over 58% for the encapsulated catalyst. For the most bulky substrate, when R = *t*Bu, the effect is less pronounced as the *ee* improves from moderate 31% to 48% (Table 2, entries 17 and 20).

Table 2. Asymmetric hydroformylation of styrene derivatives using Rh-catalysts based on **α⊂4**·$(BArF)_8$ cage structure and ligand-template system **α**(**Zn-TPP**)$_2$.[a]

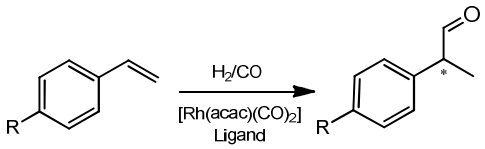

Entry	R	Cat.	b/l[b]	*ee* (%)[c]	Conv (%)	TON
1	H	**α⊂4**·$(BArF)_8$	99/1	**74 (R)**	**14**	**797**
2	H	-	*n.d.*[d]	*n.d.*[d]	<1	<1
3	H	**α**	99/1	<1	6	342
4	H	**α(Zn-TPP)$_2$**	99/1	**9(R)**	**7**	**363**
5	Cl	**α⊂4**·$(BArF)_8$	80/20	**58(R)**	**14**	**761**
6	Cl	-	*n.d.*[d]	*n.d.*[d]	<1	<1
7	Cl	**α**	91/9	<1	4	180
8	Cl	**α(Zn-TPP)$_2$**	91/9	11 (R)	12	577
9	CH_3	**α⊂4**·$(BArF)_8$	91/1	**61(R)**	**31**	**1564**
10	CH_3	-	*n.d.*[d]	*n.d.*[d]	<1	<1
11	CH_3	**α**	91/9	<1	3	140
12	CH_3	**α(Zn-TPP)$_2$**	91/9	12(R)	10	482
13	OCH_3	**α⊂4**·$(BArF)_8$	91/9	**69(R)**	**22**	**1125**
14	OCH_3	-	99/1	<1	4	180
15	OCH_3	**α**	99/1	<1.	3	168
16	OCH_3	**α(Zn-TPP)$_2$**	97/3	<1	7	340
17	^{t}Bu	**α⊂4**·$(BArF)_8$	99/1	**48(R)**	**21**	**1042**
18	^{t}Bu	-	99/1	<1	2	107
19	^{t}Bu	**α**	99/1	<1	4	180
20	^{t}Bu	**α(Zn-TPP)$_2$**	97/3	31(R)	7	361

[a] Reagents and conditions: [Rh]= 33 μM in toluene/MeCN (4/1), ligand⊂capsule /[Rh(acac)$(CO)_2$]=5, alkene/rhodium=5000, rt, 20 bar, 96 h. Rh Complex: Rh(acac)$(CO)_2$. [b] Ratio of branched and linear aldehyde. [c] Enantiomeric ratio determined by chiral GC analysis (Supelco BETA DEX 225). [d] *n.d.*= non-detected

The substrate scope was further extended to *ortho*-, *meta*- and *para*-substituted methoxystyrene derivatives to investigate the effect of steric interactions in more detail. Higher TON and ee values were obtained for *p*-methoxystyrene when **α⊂4**·$(BArF)_8$ was used as catalyst (see Table 3, entry 1), compared to the complex based on **α(Zn-TPP)$_2$** (Table 3, entry 4). In contrast, for *o*-methoxystyrene the caged catalyst gave much lower TON than the complex based on **α(Zn-TPP)**$_2$ (Table 3, entry 9 vs 12). Since *ortho*- and *para*-methoxystyrene can be considered to have electronically equivalent olefinic sites, the sharp difference is fully attributed to structural discrimination imposed by cage **4**·$(BArF)_8$. For *m*-methoxystyrene the encapsulated catalyst gave rise to a higher TON (519) than the control reaction performed with **α(Zn-TPP)$_2$** template, and the product was formed with 56 % *ee* (Table 3, entry 5). Most importantly, for *p*- and *m*-methoxystyrene the selectivity obtained for the caged catalyst was much higher than that found for the catalyst based on **α(Zn-TPP)**$_2$ (Table 3, entries 4, 8), which again clearly substantiates the importance of the catalyst confinement in the AHF of styrene.

Table 3. Asymmetric hydroformylation of *p*-, *m*- and *o*-methoxystyrene using Rh-catalysts based on **α⊂4**·$(BArF)_8$ cage structure and ligand-template system **α(Zn-TPP)**$_2$.[a]

Entry	Ligand	b/l[c]	*ee* (%)[d]	Conv (%)	TON
		para-methoxystyrene			
1	**α⊂4**·$(BArF)_8$	91/9	**69(R)**	**22**	**1125**
2	-	99/1	<1	4	180
3	**α**	99/1	<1	3	168
4	**α(Zn-TPP)$_2$**	97/3	<1	7	340
		meta-methoxystyrene			
5	**α⊂4**·$(BArF)_8$	99/1	**56**	**10**	**519**
6	-	*n.d.*[d]	*n.d.*[d].	<1	<1
7	**α**	99/1	<1	2	113
8	**α(Zn-TPP)$_2$**	99/1	<1	4	180
		ortho-methoxystyrene			
9	**α⊂4**·$(BArF)_8$	99/1	**47**	**2**	**127**
10	-	*n.d.*[d]	*n.d.*[d].	<1	<1
11	**α**	99/1	<1	2	109
12	**α(Zn-TPP)$_2$**	99/1	<1	5	245

[a] Reagents and conditions: [Rh]= 0.033 mM in toluene/MeCN (4/1), ligand⊂capsule/[Rh(acac)$(CO)_2$]=5, alkene/rhodium=5000, rt, 20 bar, 96 h. Rh Complex: Rh(acac)$(CO)_2$. [b] Ratio of branched and linear aldehyde. [c] Enantiomeric ratio determined by chiral GC analysis (Supelco BETA DEX 225). [d] *n.d.*= non-detected.

Finally, we carried out AHF catalysis of styrene at variable concentrations of **α⊂4**·$(BArF)_8$ and **α(Zn-TPP)**$_2$. We reasoned that the relative high association constant of the ligand in the cage (i.e. stability constant of **α⊂4**·$(BArF)_8$ compared to **α(Zn-TPP)**$_2$) should translate to a higher concentration window in which these supramolecular catalysts can be operated. As such, we performed experiments at four catalyst concentrations ranging from 147 to 1 μM (see Table 4). Upon lowering the concentration of Rh-**α⊂4**·$(BArF)_8$ the TON is lower as expected because of the typical positive order of the catalyst concentration on the reaction rate. Most indicative

for the stability of the assembly is the selectivity. The selectivity induced by the encapsulated catalysts remains high (71 ± 3% *ee*) even at concentrations of 6 μM, indicating that under these conditions the catalysis is still dominated by the encapsulated catalyst (see Figure S30). In contrast, when Rh-**α**(**Zn-TPP**)$_2$ catalyst was used at 6 μM the product was formed in racemic form, and also the TON was similar to the control experiment where no porphyrins were present. These results are in agreement with a significantly more robust nature of catalyst **α**⊂**4**·(BArF)$_8$ compared to **α**(**Zn-TPP**)$_2$.

Table 4. Asymmetric hydroformylation of styrene at different Rh-catalyst concentrations.[a]

Entry	Cat.	[Rh] (μM)	b/l[b]	*ee* (%)[c]	Conv (%)	TON
1	**α**⊂**4**·(BArF)$_8$	147	98/2	**71**	**97**	**193**
2	-		96/4	<1	64	128
3	**α**		98/2	3	90	180
4	**α**(**Zn-TPP**)$_2$		97/3	**15**	**92**	**183**
5	**α**⊂**4**·(BArF)$_8$	33	97/3	**68**	**79**	**158**
6	-		91/9	<1	20	39
7	**α**		97/3	3	88	176
8	**α**(**Zn-TPP**)$_2$		97/3	16	49	99
9	**α**⊂**4**·(BArF)$_8$	6	99/1	74	14	29
10	-		-	*n.d*[d]	0	0
11	**α**		99/1	<1	17	33
12	**α**(**Zn-TPP**)$_2$		99/1	<1	15	31
13	**α**⊂**4**·(BArF)$_8$	1	-	*n.d*[d]	0	0
14	-		-	*n.d*[d]	0	0
15	**α**		-	*n.d*[d]	0	0
16	**α**(**Zn-TPP**)$_2$		-	*n.d*[d]	0	0

[a] Reagents and conditions: toluene/MeCN (4/1), ligand⊂capsule/[Rh(acac)(CO)$_2$]=5, alkene/rhodium=200, rt, 20 bar, 96 h. Rh Complex: Rh(acac)(CO)$_2$. [b] Ratio of branched and linear aldehyde. [c] Enantiomeric ratio determined by chiral GC analysis (Supelco BETA DEX 225).[d] *n.d.*= non-detected.

Conclusion

In summary, this work describes the encapsulation of a monoligated chiral rhodium complex in a self-assembled molecular cage. The encapsulated Rh-**α**⊂**4**·$(BArF)_8$ catalyst exhibits among the highest selectivities in the asymmetric hydroformylation of styrenes for monoligated rhodium catalysts.[6] Most significantly, stereoselectivity observed in the hydroformylation of styrenes upon encapsulation of the catalyst are substantially improved with regard to analogous reactions performed with the catalyst operating in bulk solution. Therefore, the cage can be considered as a second coordination sphere of the catalyst, and its role may be understood as reminiscent of enzymatic active sites. On the basis of these observations, we envision that the use of the second coordination sphere tuning strategy over the selectivity of catalytic events may be more broadly applicable. The size-tunability of cage **4**·$(BArF)_8$, the high affinity for pyridine-containing ligands and the possibility to modify the apertures of the cage provide strong fundaments for the future development of these cage structures for asymmetric catalysis.

Experimental Section

Materials. Unless indicated otherwise, reagents and solvents used were commercially available reagent quality and reactions were carried out under an atmosphere of nitrogen using standard Schlenk techniques. Ligands **α**[14], **β**[10] and molecular cage **4**·$(BArF)_8$[33] were synthesized following previously reported procedures.

Physical Methods. NMR spectra (^1H, ^{31}P and ^{13}C) were measured on a Bruker DRX 400 MHz, Bruker AVANCE 500 MHz, Bruker AVANCE 600 MHz and Varian Inova 500 MHz; $CDCl_3$, CD_3CN or Toluene-d_8 were used as solvents, if not further indicated. High resolution mass spectra (HRMS) were obtained on a Bruker MicroTOF-Q-II, using acetonitrile as the mobile phase. UV-Vis spectroscopy was performed on an Agilent 8452 UV-vis spectrophotometer with 1 cm quartz cell. Gas chromatographic analyses were runed on a Shimadzu GC-17A apparatus (split/splitless injector, J&W 30 m column, film thickness 3.0 μm, carrier gas 70kPa He, FID Detector). Chiral GC separations were conducted on the Iterscience HR GC with a Supelco β-dex 225 capillary column. IR experiments were performed at r.t. into a Nicolet 510 FTIR spectrometer. Molecular Modeling calculations were performed using PM3-Spartan molecular modeling program.

Synthesis of ligands γ and δ. In a flame dried Schlenk 200 mg (0.44 mmol) **d**, pyridine (0.068 mL, 0.88 mmol) and DMAP (10 mol%) were suspended in dry toluene (4.4 mL, 0.1 M). The solution was cooled to 0 °C and distilled PCl_3 (0.080 mL, 0.88 mmol) was added dropwise over 10 min. The mixture was warmed up to room temperature and then refluxed overnight. The

reaction mixture was cooled to room temperature and the formation of product was checked by ^{31}P-NMR. The solvent and the residual PCl_3 were removed in vacuum. The resulting solid was used for the next step without any further purification.

In a flame dried Schlenk the dialkylamine (0.44 mmol) and pyridine (0.040 mL, 0.48 mmol) were dissolved in dry toluene (1 mL). The solution was added drop wise to a cooled (0 °C) mixture of **e** (225.7 mg, 0.44 mmol) in dry toluene (5 mL). The mixture was warmed up to room temperature and stirred overnight at room temperature. The precipitate formed was filtered over a pad of Celite under argon, and then solvent was evaporated in vacuum to obtain **α**, **γ**, **δ**.

See reaction scheme (including **a**-**e** representations) in the supporting information. See also Figures S31-32.

Ligand **γ**: Yield: 81 % (white foam); ^{1}H NMR (400 MHz, $CDCl_3$): δ = 8.85 (m, 2H) 8.54 (dd, 2H), 7.96 (dt, 1H), 7.90 (dt, 1H), 7.28 (m, 2H), 7.16 (s, 1H), 7.14 (s, 1H), 2.90 (m, 4H), 2.54 (m, 2H), 2.35 (m, 4H), 1.87 (m, 8H), 0.51-0.59 (t, 6H); ^{13}C NMR: 150.2, 149.1, 147.2, 138.0, 136.2, 130.2, 129.1, 128.4, 122.5, 122.1, 34.2, 30.2, 29.1, 28.3, 27.8, 23.1, 22.2; ^{31}P NMR: δ= 140.85 ppm.

Ligand **δ**: Yield: 52 % (white foam); ^{1}H NMR (400 MHz, Toluene): δ = 8.99-9.07 (dd, 2H) 8.43 (d, 2H), 7.84 (dt, 1H), 7.73 (dt, 1H), 7.01 (m, 2H), 6.97 (s, 1H), 6.71 (s, 1H), 2.68 (m, 6H), 2.44 (m, 2H), 1.79 (m, 2H), 1.59 (m, 8H), 0.87 (4*d, 12H); ^{13}C NMR: 153.2, 152.7,150.2, 14.1, 139.2, 138.0, 135.2, 130.2, 129.1, 128.6, 122.1, 47.5, 46.6, 35.6, 34.2, 31.1, 28.3, 12.8, 12.1, 11.2; ^{31}P NMR: δ= 139.89 ppm.

Preparation of 4,4'-bpy⊂4·(BArF)$_8$.[33] 4.0 mg of **4**·$(BArF)_8$ nanocapsule (0.33 μmols, 1 equiv.) were dissolved in 100 μl of CH_3CN. Then 1 equiv. of 4,4'-Bpy dissolved in 400 μl of toluene was added. The mixture was stirred at room temperature for 5 minutes. After the reaction time, the mixture was filtered through cotton and recrystallized by diethyl ether diffusion. Quantitative yield obtained. ^{1}H-NMR (400 MHz, CD_3CN) δ ppm: 8.59 (s, 16H, pyrrole ring), 8.58 (dd, 8 H, arom-porph), 8.34 (dd, J=8 Hz, 8H, arom-porph), 8.28 (d, J= 8.5 Hz, 32 H, arom-clip), 8.13 (m, 32 H arom-clip + 8H arom-porph), 7.99 (dd, J=8 Hz, 8H, arom-porph), 7.67 (m, 96 H, NaBARF)*, 4.95 (m, 4 H, bpy) 4.04 (d, J=13 Hz, 16 H, -CH_2-), 3.73 (m, 16H, -CH_2-), 3.60 (s, 48 H, N-CH_3), 3.37 (m, 16 H, -CH_2-), 3.14 (d, J=13 Hz, 16 H, -CH_2-), 2.48 (dd, J=13.5, 16 H, -CH_2-), 2.38 (dd, J=13.5, 16 H, -CH_2-), 1.59 (s, 24 H, N-CH_3). HRMS (m/z): calcd. 2186.923 and found 2186.910 ({**4,4'-bpy⊂4**·$(BArF)_4$}$^{4+}$); calcd. 1577.118 and found 1577.115 ({**4,4'-bpy⊂4**·$(BArF)_3$}$^{5+}$), calcd. 1170.251 and found 1170.255 ({**4,4'-bpy⊂4**·$(BArF)_2$}$^{6+}$); calcd. 879.634 and found 879.637 ({**4,4'-bpy⊂4**·(BArF)}$^{7+}$); calcd. 661.796 and found 661.799 ({**4,4'-bpy⊂4**·(BArF)}$^{8+}$).

Preparation of α⊂4·(BArF)$_8$. 9 mg of **4**·(BArF)$_8$ nanocapsule (0.33 μmols, 1 equiv.) were dissolved in 300 μl of CH_3CN. Then 1 equiv. of **α** dissolved in 1200 μl toluene was added. The mixture was stirred at room temperature for 5 minutes. After the reaction time, the mixture is filtered through cotton and recrystallized by diethyl ether diffusion. Quantitative yield obtained. HRMS (m/z): calcd. 2278.453 and found 2278.452 ({**α⊂4**·(BArF)$_4$}$^{4+}$); calcd. 1650.120 and found 1650.151 ({**α⊂4**·(BArF)$_3$}$^{5+}$), calcd. 1231.231 and found 1231.283 ({**α⊂4**·(BArF)$_2$}$^{6+}$); calcd. 931.942 and found 931.945 ({**α⊂4**·(BArF)}$^{7+}$); calcd. 707.621 and found 707.693 ({**α⊂4**·(BArF)}$^{8+}$).

Preparation of the *trans*-[Rh(H)(CO)$_3$-α⊂4·(BArF)$_8$ complex for the high pressure NMR experiment. To 16 mg of **4**·(BarF)$_8$ (0.0013 μmol), 1 eq the phosphoramidite ligand (α, β, γ or δ), 1 eq Rh(acac)(CO)$_2$ were added in a 7/3 (v/v) mixture of d_8-Toluene/CD_3CN (1.2 ml). The mixture was transferred into a 5 mm HP-NMR tube, pressurized with 5 bar of syngas H_2/CO_2 1:1, and left at 40ºC for 16 h. After this time the High pressure NMR spectra was recorded.

Diffusion-Ordered NMR spectroscopy experiments. Diffusion-Ordered NMR experiment (DOSY NMR) allows the determination of the translational self-diffusion coefficients (*D*) for these species in acetonitrile solution. Making use of the Stokes-Einstein equation (SEq.1), the hydrodynamic radii (r_h) for the diffused species can be calculated from the *D* value.[42]

$$D = \frac{k \cdot T}{6 \cdot \pi \cdot \eta \cdot r_H} \qquad \text{(SEq.1)}$$

where k is the Boltzmann constant, T is the temperature, and η is the viscosity of the solvent (η (CH_3CN) = 0.35 mPa s).

General procedure for UV-Vis titrations. Host-guest interactions in solution were studied by UV-Vis spectroscopy. Solutions of nanocapsule **4**·(BArF)$_8$ ($4.32 \cdot 10^{-7}$ M) and of the different substrates tested ($1.39 \cdot 10^{-5}$ M) were prepared using CH_3CN/Tol (1/9) as solvent. An increasing number of substrate equivalents were added to the nanocapsule solution (2ml, in a 1cm cuvette cell). The host concentration was kept constant. The stoichiometry of the complexes was studied using the method of Continuous Variations, by adding different ratios of guest solution, in order to add an increasing number of substrate equivalents.

Hydroformylation Catalysis Unless indicated otherwise, the hydroformylation experiments were carried out in a stainless stell autoclave charged with an inset suitable for 8 reaction vessels (equiped with teflon mini stirring bars) for performing parallel reactions. Each vial was charged with phosphoramidite ligands (**α, β**, **γ**, **δ**, 0.083 μmols), the template **Zn-TPP** (0.166 μmols) or nanocapsule **4**·(BArF)$_8$ (0.083 μmols), [Rh(acac)CO_2] (0.016 μmols), the substrate (83 μmols) and a mixture of toluene/acetonitrile (v/v, 4/1). The substrates were filtrated

through basic alumina to remove possible peroxide immpurities.The solvents were destilled from sodium previous to use. Before starting the catalysis, the charged autoclave was purged three times with 10 bar of syngas (H_2/CO=1/1) and then pressurized to 20 bar. After the catalytic reaction, the autoclave was cooled to r.t. if the reaction was carried out at high temperature, the pressure was reduced to 1.0 bar and a few drops of tri-butyl-posphite were added in each reaction vessel to prevent any further reaction. The reaction mixtures were not filtered over basic alumina to remove the catalyst residues, because filtration may cause retention of the aldehydes influencing the GC results. The mixtures were diluted with CH_2Cl_2 for GC analysis. The enantiomeric excess was analyzedby GC (Supelco β-dex 225 capillary column). The absolute configuration was determined by comparing the chiral GC traces of the reaction mixture with the comercially abailable enantiopure aldehydes.

Associated content.

Supporting information. DOSY 2D experiments of **4,4'-bpy⊂4**·$(BArF)_8$. All 1D and 2D NMR spectra. HRMS results. UV-Vis experiments. Chiral GC data for hydroformylation products information and chromatograms (Figures S33-37). This material is available free of charge via the Internet at http://pubs.acs.org.

Acknowledgments.

We would like to acknowledge the European Research Council (ERC-2011-StG-277801 to XR, ERC-2009-StG-239910 to MC and ERC-2013-AdG-339782-NAT_CAT to JNHR), the Spanish MINECO (Consolider-Ingenio CSD2010-00065, INNPLANTA project INP-2011-0059-PCT-420000-ACT1, CTQ2012-32436) and the Catalan DIUE of the Generalitat de Catalunya (2009SGR637 and PhD grant to CGS). XR and MC also thank ICREA-Acadèmia awards.

Bibliography

1. Reetz, M. T., *Angew. Chem. Int. Ed.* **2011**, *50*, 138-174.
2. Dang, D.; Wu, P.; He, C.; Xie, Z.; Duan, C., *J. Am. Chem. Soc.* **2010**, *132*, 14321-14323.
3. Banerjee, M.; Das, S.; Yoon, M.; Choi, H. J.; Hyun, M. H.; Park, S. M.; Seo, G.; Kim, K., *J. Am. Chem. Soc.* **2009**, *131*, 7524-7525.
4. Zhang, Y.; Wang, S.; Enright, G. D.; Breeze, S. R., *J. Am. Chem. Soc.* **1998**, *120*, 9398-9399.
5. Stang, P. J.; Olenyuk, B., *Angew. Chem. Int. Ed.* **1996**, *35*, 732-6.
6. Jouffroy, M.; Gramage-Doria, R.; Armspach, D.; Sémeril, D.; Oberhauser, W.; Matt, D.; Toupet, L., *Angew. Chem. Int. Ed.* **2014**, *53*, 3937-3940.
7. Lee, S. J.; Cho, S.-H.; Mulfort, K. L.; Tiede, D. M.; Hupp, J. T.; Nguyen, S. T., *J. Am. Chem. Soc.* **2008**, *130*, 16828-16829.
8. Kuil, M.; Goudriaan, P. E.; van Leeuwen, P. W. N. M.; Reek, J. N. H., *Chem. Commun.* **2006**, 4679-4681.
9. Kuil, M.; Goudriaan, P. E.; Kleij, A. W.; Tooke, D. M.; Spek, A. L.; van Leeuwen, P. W. N. M.; Reek, J. N. H., *Dalton Trans.* **2007**, 2311-2320.

10. Bellini, R.; Chikkali, S. H.; Berthon-Gelloz, G.; Reek, J. N. H., *Angew. Chem. Int. Ed.* **2011**, *50*, 7342-7345.
11. Bellini, R.; Reek, J. N. H., *Chem. Eur. J.* **2012**, *18*, 7091-7099.
12. Bellini, R.; Reek, J. N. H., *Chem. Eur. J.* **2012**, *18*, 13510-13519.
13. Bellini, R.; Reek, J. N. H., *Eur. J. Inorg. Chem.* **2012**, *2012*, 4684-4693.
14. Gadzikwa, T.; Bellini, R.; Dekker, H. L.; Reek, J. N. H., *J. Am. Chem. Soc.* **2012**, *134*, 2860-2863.
15. Yoshizawa, M.; Tamura, M.; Fujita, M., *Science* **2006**, *312*, 251-254.
16. Pluth, M. D.; Bergman, R. G.; Raymond, K. N., *Science* **2007**, *316*, 85-88.
17. Yoshizawa, M.; Klosterman, J. K.; Fujita, M., *Angew. Chem. Int. Ed.* **2009**, *48*, 3418-3438.
18. Pluth, M. D.; Bergman, R. G.; Raymond, K. N., *Acc. Chem. Res.* **2009**, *42*, 1650-1659.
19. Kleij, A. W.; Reek, J. N. H., *Chem. Eur. J.* **2006**, *12*, 4218-4227.
20. Pemberton, B. C.; Raghunathan, R.; Volla, S.; Sivaguru, J., *Chem. Eur. J.* **2012**, *18*, 12178-12190.
21. Koblenz, T. S.; Wassenaar, J.; Reek, J. N. H., *Chem. Soc. Rev.* **2008**, *37*, 247-262.
22. Raynal, M.; Ballester, P.; Vidal-Ferran, A.; van Leeuwen, P. W. N. M., *Chem. Soc. Rev.* **2014**, *43*, 1734-1787.
23. Breiner, B.; Clegg, J. K.; Nitschke, J. R., *Chem. Sci.* **2011**, *2*, 51-56.
24. Wiester, M. J.; Ulmann, P. A.; Mirkin, C. A., *Angew. Chem. Int. Ed.* **2011**, *50*, 114-137.
25. Leenders, S. H. A. M.; Gramage-Doria, R.; de Bruin, B.; Reek, J. N. H., *Chem. Soc. Rev.* **2015**, *DOI: 10.1039/C4CS00192C*.
26. Brown, C. J.; Bergman, R. G.; Raymond, K. N., *J. Am. Chem. Soc.* **2009**, *131*, 17530-17531.
27. Zhao, C.; Sun, Q.-F.; Hart-Cooper, W. M.; DiPasquale, A. G.; Toste, F. D.; Bergman, R. G.; Raymond, K. N., *J. Am. Chem. Soc.* **2013**, *135*, 18802-18805.
28. Zhao, C.; Toste, F. D.; Raymond, K. N.; Bergman, R. G., *J. Am. Chem. Soc.* **2014**, *136*, 14409-14412.
29. Slagt, V. F.; Reek, J. N. H.; Kamer, P. C. J.; Leeuwen, P. W. N. M. V., *Angew. Chem. Int. Ed. Engl.* **2001**, *40*, 4271-4274.
30. Slagt, V. F.; Kamer, P. C. J.; Leeuwen, P. W. N. M. v.; Reek, J. N. H., *J. Am. Chem. Soc.* **2004**, *126*, 1526-1536.
31. Kuil, M.; Soltner, T.; Leeuwen, P. W. N. M. v.; Reek, J. N. H., *J. Am. Chem. Soc.* **2006**, *128*, 11344-11345
32. Bocokić, V.; Kalkan, A.; Lutz, M.; Spek, A. L.; Gryko, D. T.; Reek, J. N. H., *Nat. Commun.* **2013**, *4*, 2670.
33. García-Simón, C.; Garcia-Borràs, M.; Gómez, L.; Parella, T.; Osuna, S.; Juanhuix, J.; Imaz, I.; Maspoch, D.; Costas, M.; Ribas, X., *Nat Commun* **2014**, *5*, 5557.
34. O'Sullivan, M. C.; Sprafke, J. K.; Kondratuk, D. V.; Rinfray, C.; Claridge, T. D. W.; Saywell, A.; Blunt, M. O.; O'Shea, J. N.; Beton, P. H.; Malfois, M.; Anderson, H. L., *Nature* **2011**, *469*, 72-75.
35. Pazderski, L., *Magn. Reson. Chem.* **2008**, *46*, S3-S15.
36. Kline, M.; Cheatham, S., *Magn. Reson. Chem.* **2003**, *41*, 307-314.
37. Franke, R.; Selent, D.; Boerner, A., *Chem. Rev.* **2012**, *112*, 5675-5732.
38. Agbossou, F.; Carpentier, J. F.; Mortreux, A., *Chem. Rev.* **1995**, *95*, 2485-2506.
39. Dieguez, M.; Pàmies, O.; Claver, C., *Tetrahedron: Asymmetry* **2004**, *15*, 2113-2122.
40. Klosin, J.; Landis, C. R., *Acc. Chem. Res.* **2007**, *40*, 1251-1259.
41. Chikkali, S. H.; Vlugt, J. L. v. d.; Reek, J. N. H., *Coord. Chem. Rev.* **2014**, *262*.
42. Ribas, X.; Dias, J. C.; Morgado, J.; Wurst, K.; Almeida, M.; Parella, T.; Veciana, J.; Rovira, C., *Angew. Chem. Int. Ed.* **2004**, *43*, 4049-4052.

Table of contents